Navigation, Guidance and Control of AUVs: An Application to the MARIUS Vehicle *

D. Fryxell †, P. Oliveira †, A. Pascoal †, C.Silvestre †and I. Kaminer ‡

†- Institute for Systems and Robotics and Department of Electrical Engineering
Instituto Superior Técnico, Av. Rovisco Pais, 1096 Lisboa Codex, Portugal
‡- Department of Aeronautics and Astronautics, Naval Postgraduate School
Monterey, California 93943, USA

Abstract. This paper addresses the problem of designing guidance, control and navigation systems for autonomous underwater vehicles (AUVs). Its contribution is twofold: i) it introduces a new methodology for integrated design of guidance and control, and ii) it describes a novel approach to the analysis and design of multi-rate complementary filters for navigation. The methodologies proposed lead to an efficient procedure for the design of controllers for AUVs to accurately track reference trajectories defined in an inertial reference frame. The paper illustrates the application of this procedure to the design of a tracking controller for the AUV MARIUS. The design phase is summarized, and the performance of the resulting controller is assessed in simulation using dynamic models of the vehicle and its sensor suite.

Key Words. AUVs, Guidance, Navigation, Control, Gain Scheduling.

1 Introduction. Guidance, Control and Navigation

In a great number of envisioned mission scenarios, Autonomous Underwater Vehicles (AUVs) will be required to follow inertial reference trajectories accurately ["Pascoal (1994)"]. To achieve that goal, the following systems must be designed and implemented on-board AUVs: i) *navigation*, to provide estimates of linear and angular positions and velocities of the vehicle, ii) *guidance*, to process navigation/inertial reference trajectory data and output set-points for the vehicle's (body) velocity and attitude, and iii) *control*, to generate the actuator signals that are required to drive the actual velocity and attitude of the vehicle to the values commanded by the guidance scheme.

Traditionally, control and guidance systems are designed separately, using well established design methods for control and simple strategies such as line of sight (LOS) for guidance, see ["Healey (1993)"] and the references therein. During the design phase, the control system is usually designed with sufficiently large bandwidth to track the commands that are expected from the guidance system. However, since the two systems are effectively coupled, stability and adequate performance of the combined system about nominal trajectories are not guaranteed. In practice, this problem can be resolved by judicious choice of guidance law parameters (such as so-called visibility distance in LOS strategy), based on extensive computer simulations. Even when stability is obtained, however, the resulting strategy leads to finite trajectory tracking errors, the magnitude of which depends on the type of trajectory to be tracked (radius of curvature, vehicle's desired speed, etc,).

The first part of the paper proposes a new methodology for the design of guidance and control systems for AUVs, whereby the two systems are effectively designed simultaneously. The key idea is to realize that for these types of vehicles the equilibrium (also known as trimming) trajectories are helices parameterized by the vehicle's body axis velocity, yaw rate and flight path angle. Furthermore, using a convenient coordinate transformation, the linearization of the vehicle error dynamics and kinematics about any trimming trajectory can be shown to be time-invariant ["Silvestre (1994)"]. Thus, the problem of designing integrated guidance/control systems to track inertial trajectories that consist of the piecewise union of trimming trajectories, falls within the scope of gain scheduled control theory ["Kaminer (1993)"]. Using this approach, the vehicle's body axis velocity, yaw rate, and flight path angle play the role of scheduling variables that interpolate the parameters of linear controllers designed for a finite number of representative trimming trajectories. The results reported in ["Kaminer (1993)"] on so-called *D*-implementation
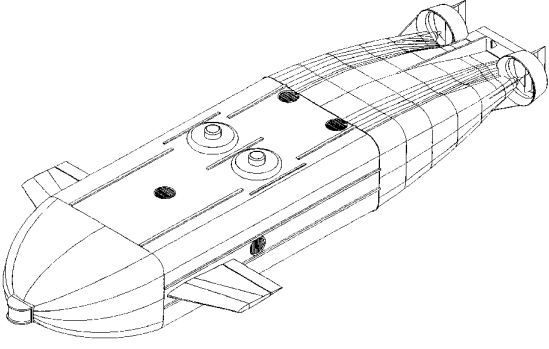
Figure 1.1: The vehicle MARIUS

of gain scheduled controllers can then be used to obtain a combined guidance/control system such that the properties of the linear designs are recovered locally, about each trimming trajectory. This new approach guarantees that the steady state tracking error about any trimming trajectory condition is zero. Moreover, the D-implementation method leads naturally to a structure where the only exogenous commands required are the desired linear inertial position and yaw rate, thus avoiding the need to feedforward the trimming conditions for the remaining state variables. Due to space limitations, the methodology used for the design of combined guidance and control systems for the AUV MARIUS is only briefly summarized here. For complete details, see ["Silvestre (1994)"].

The second part of the paper describes the design of the navigation system for the AUV MARIUS using a conceptually simple framework for filtering that is rooted in the kinematic equations of motion of the vehicle. This approach borrows from complementary filtering theory, see ["Lin (1991)"] for an introduction to the subject and for interesting applications to aircraft navigation. The setup adopted leads naturally to the design of linear Kalman filters, whereby the covariances of process and observation noises are viewed as tuning knobs to shape the characteristics of the operators that map measured into estimated variables. In the case of attitude estimation, all sensors are sampled at the same rate and the corresponding operators are linear time-invariant. This leads to an interpretation of the filters in the frequency domain that is fruitful in analyzing the stability of combined guidance, control and navigation ["Oliveira (1994)"]. In the case of linear position and velocity estimation, however, the characteristics of the sound channel imply that the position measurements (obtained from a long baseline system) are available at a rate that is lower than that of the remaining sensors. This problem has been tackled in ["Oliveira (1994)"], where a new approach to the design and analysis of multi-rate complementary filters was introduced. Interestingly enough, these filters can be viewed as input-output operators that exhibit "frequency-like" properties that are the natural generalization of those obtained for the single rate case.

The paper is organized as follows: Section 2 introduces the model of the AUV MARIUS and derives its linearized equations of motion about trimming trajectories. Section 3 describes the structure of a gain scheduled trajectory tracking controller for the vehicle. Section 4 describes the AUV's multi-rate navigation system. Finally, Section 5 assesses the performance of combined navigation, guidance and control in simulation.

2 Vehicle Dynamics.

This section describes the dynamic model of the AUV MARIUS, depicted in figure 1.1. A complete study of the AUV dynamics based on hydrodynamic tank tests with a Planar Motion Mechanism (PMM) can be found in ["Fryxell (1994)"]. In what follows, $\{I\}$ denotes a universal reference frame, and $\{B\}$ denotes a body-fixed coordinate frame that moves with the AUV. The following notation is required:

$\mathbf{p} = [x,\ y,\ z]'$ - position of the origin of $\{B\}$ expressed in $\{I\}$;

$\mathbf{v} = [u,\ v,\ w]'$ -linear velocity of the origin of $\{B\}$ relative to $\{I\}$, expressed in $\{B\}$;

$\boldsymbol{\lambda} = (\phi,\ \theta,\ \psi)'$ - vector of Euler angles which describe the orientation of frame $\{B\}$ with respect to $\{I\}$

$\boldsymbol{\omega} = [p,\ q,\ r]'$ - angular velocity of $\{B\}$ relative to $\{I\}$, expressed in $\{B\}$;

$\mathbf{R} = \mathbf{R}(\boldsymbol{\lambda})$ - rotation matrix from $\{B\}$ to $\{I\}$.

$\mathbf{Q} = \mathbf{Q}(\boldsymbol{\lambda})$ - matrix that relates $\boldsymbol{\lambda}$ to $\boldsymbol{\omega}$ and satisfies $\dot{\boldsymbol{\lambda}} = \mathbf{Q}(\boldsymbol{\lambda})\boldsymbol{\omega}$.

The symbol $\boldsymbol{\delta} := [\delta_{a,c}, \delta_{a,d}, \delta_e, \delta_r]'$ denotes the vector whose entries correspond to deflections of the ailerons (common and differential), elevator, and rudder, respectively and the symbol n denotes the propeller rotational rate. With the above notation, the dynamics of the AUV can be written in compact form as

$$M_{RB}\ddot{\mathbf{q}} + C_{RB}(\dot{\mathbf{q}})\dot{\mathbf{q}} = \boldsymbol{\tau}(\ddot{\mathbf{q}}, \dot{\mathbf{q}}, \boldsymbol{\lambda}, \boldsymbol{\delta}, n), \qquad (2.1)$$

where $\boldsymbol{\tau}$ denotes the vector of external forces, $\dot{\mathbf{q}} = [\mathbf{v}', \boldsymbol{\omega}']'$, and M_{RB} and C_{RB} denote the rigid body inertia matrix and the matrix of Coriolis and centrifugal terms, respectively. The vector $\boldsymbol{\tau}$ can further be decomposed as

$$\boldsymbol{\tau}(\ddot{\mathbf{q}}, \dot{\mathbf{q}}, \boldsymbol{\lambda}, \boldsymbol{\delta}, n) = \boldsymbol{\tau}_{rest}(\boldsymbol{\lambda}) + \boldsymbol{\tau}_{add}(\ddot{\mathbf{q}}, \dot{\mathbf{q}}) \quad (2.2)$$
$$+ \boldsymbol{\tau}_{lift}(\dot{\mathbf{q}}, \boldsymbol{\delta}) + \boldsymbol{\tau}_{visc}(\dot{\mathbf{q}}, \boldsymbol{\delta}) + \boldsymbol{\tau}_{prop}(n),$$

where $\boldsymbol{\tau}_{rest}$ denotes the forces and moments caused by gravity and buoyancy and $\boldsymbol{\tau}_{add}$ is the added mass term. The term $\boldsymbol{\tau}_{lift}$ captures the effects of the lifting forces generated by the deflecting surfaces, $\boldsymbol{\tau}_{visc}$ consists of the forces and moments caused by skin friction, and $\boldsymbol{\tau}_{prop}$ represents the forces and moments generated by the main propellers. Using equation (2.1) and the associated kinematic relationships, the state space model for the AUV can be written as

$$\mathcal{G} = \begin{cases} \ddot{\mathbf{q}} = F(\dot{\mathbf{q}}, \boldsymbol{\lambda}) + G(\dot{\mathbf{q}})H(\dot{\mathbf{q}}, \mathbf{u}) \\ \dot{\mathbf{p}} = \mathbf{R}\,\mathbf{v} \\ \dot{\boldsymbol{\lambda}} = \mathbf{Q}\,\boldsymbol{\omega}, \end{cases} \qquad (2.3)$$

where F, G and H are continuously differentiable functions, $\mathbf{v}$, $\boldsymbol{\omega}$, $\mathbf{p}$ and $\boldsymbol{\lambda}$ are state space variables, and $\mathbf{u} = [\boldsymbol{\delta}', n]'$ is the vector of control inputs. An equilibrium or trimming trajectory of (2.3) is defined as a path $\mathcal{P}_c = [\dot{\mathbf{q}}_C', \mathbf{p}_C', \boldsymbol{\lambda}_C{}']'$ such that

$$F(\dot{\mathbf{q}}_C, \boldsymbol{\lambda}_C) + G(\dot{\mathbf{q}}_C)H(\dot{\mathbf{q}}_C, \mathbf{u}_C) = 0 \qquad (2.4)$$

for some constant vector $\mathbf{u}_C$. Notice that for simplicity, the equations do not show the explicit dependence on time.

From equation (2.1), it can be concluded that the only possible trimming trajectories $\mathcal{P}_c$ correspond to helices defined by

$$\dot{\boldsymbol{\lambda}}_C = \begin{bmatrix} 0 \\ 0 \\ \dot{\psi}_C \end{bmatrix}, \quad \dot{\mathbf{p}}_C = \begin{bmatrix} \mathbf{V}_{T_c} \cos(\gamma_C) \cos(\dot{\psi}_C t) \\ \mathbf{V}_{T_c} \cos(\gamma_C) \sin(\dot{\psi}_C t) \\ -\mathbf{V}_{T_c} \sin(\gamma_C) \end{bmatrix},$$

(2.5)

where $\dot{\psi}_C$ is yaw rate, $\mathbf{V}_{T_c} = \|\mathbf{v}_C\|$ is body linear speed and γ_C is so-called flight path angle. Thus, the trimming trajectories can be parameterized by the vector $\alpha_c = [\mathbf{V}_{T_c}, \dot{\psi}_C, \gamma_C] \in \mathcal{R}^3$.

Given α_c, the corresponding trimming values for the state variables of (2.3) can be determined from analytical and numerical computations, as follows. Let $G^{\perp}(\dot{\mathbf{q}})$ be the orthogonal complement of $G(\dot{\mathbf{q}})$ satisfying $G^{\perp}(\dot{\mathbf{q}})G(\dot{\mathbf{q}}) = 0$. Multiplying the first equation of (2.3) by $G^{\perp}(\dot{\mathbf{q}})$, it follows that

$$\begin{cases} 0 = G^{\perp}(\dot{\mathbf{q}}_C)F(\dot{\mathbf{q}}_C, \boldsymbol{\lambda}_C) \\ \dot{\mathbf{p}}_C = \mathbf{R}_C \, \mathbf{v}_C \\ \dot{\boldsymbol{\lambda}}_C = \mathbf{Q}_C \, \boldsymbol{\omega}_C \end{cases} \qquad (2.6)$$

along a trimming trajectory, thus eliminating the control input $\mathbf{u}_C$. By requiring that $\delta_{a,c} = 0$ at trimming, it can be shown that (2.6), together (2.5), provide a set of equations that can be solved numerically to give $\mathbf{v}, \boldsymbol{\omega}, \phi, \theta$ as functions of $\mathbf{V}_{T_c}, \gamma_C, \dot{\psi}_C$, thus concluding the computation of all relevant state variables at trimming. For complete details, the reader is referred to ["Silvestre (1994)"]. In what follows, the symbol $\mathcal{P}_c(\alpha_c)$ denotes a path parameterized by α_c.

Let $\mathcal{P}_c(\alpha_c)$ be a trimming trajectory for the vehicle, and define the variables

$$\begin{cases} \mathbf{v}_E = \mathbf{v} - \mathbf{v}_C \\ \boldsymbol{\omega}_E = \boldsymbol{\omega} - \boldsymbol{\omega}_C \\ \mathbf{p}_E = \mathbf{R}^{-1}(\mathbf{p} - \mathbf{p}_C) \\ \boldsymbol{\lambda}_E = \mathbf{Q}^{-1}(\boldsymbol{\lambda} - \boldsymbol{\lambda}_C), \end{cases} \qquad (2.7)$$

which can be interpreted as the generalized error vector between the vehicle state and the trajectory $\mathcal{P}_c(\alpha_c)$. Let $\mathbf{u}_E = \mathbf{u} - \mathbf{u}_C$. By noticing that $\mathbf{v}_C$ and $\boldsymbol{\omega}_C$ are constant along trimming trajectories, straightforward computations show that

$$\begin{cases} \ddot{\mathbf{q}}_E = \mathcal{F}(\dot{\mathbf{q}}_E, \boldsymbol{\lambda}_E) + \mathcal{G}(\dot{\mathbf{q}}_E)\mathcal{H}(\dot{\mathbf{q}}_E, \mathbf{u}_E) \\ \dot{\mathbf{p}}_E = \mathbf{v}_E + \mathbf{v}_C - \mathbf{R}_C^{-1}\mathbf{R}\,\mathbf{v}_C - S(\boldsymbol{\omega}_E + \boldsymbol{\omega}_C)\mathbf{p}_E \\ \dot{\boldsymbol{\lambda}}_E = \boldsymbol{\omega}_E + \boldsymbol{\omega}_C - \mathbf{Q}^{-1}\mathbf{Q}_C\,\boldsymbol{\omega}_C + \dot{\mathbf{Q}}^{-1}\,\mathbf{Q}\,\boldsymbol{\lambda}_E, \end{cases}$$

(2.8)

where

$$\begin{aligned} \mathcal{F}(\dot{\mathbf{q}}_E, \boldsymbol{\lambda}_E) &= F(\dot{\mathbf{q}}_E + \dot{\mathbf{q}}_C, \mathbf{Q}\,\boldsymbol{\lambda}_E + \boldsymbol{\lambda}_C) \\ \mathcal{G}(\dot{\mathbf{q}}_E) &= G(\dot{\mathbf{q}}_E + \dot{\mathbf{q}}_C) \\ \mathcal{H}(\dot{\mathbf{q}}_E, \mathbf{u}) &= H(\dot{\mathbf{q}}_E + \dot{\mathbf{q}}_C, \mathbf{u}_E + \mathbf{u}_C), \end{aligned}$$

and $S(\boldsymbol{\omega})$ is the skew-symmetric matrix defined by $S(\boldsymbol{\omega}) = \boldsymbol{\omega}\times$. It is now possible to prove that the linearization of (2.8) about the error vector $[0'_{12\times 1}\mathbf{u}'_C]'$ is *time-invariant* and can be written in the form

$$\begin{cases} \delta\ddot{\mathbf{q}}_E = A_{\dot{\mathbf{q}}_E}(\alpha_c)\delta\dot{\mathbf{q}}_E + A_{\boldsymbol{\lambda}_E}(\alpha_c)\delta\boldsymbol{\lambda}_E + B(\alpha_c)\delta\mathbf{u}_E \\ \delta\dot{\mathbf{p}}_E = \delta\mathbf{v}_E - S(\boldsymbol{\omega}_C)\delta\mathbf{p}_E - S(\mathbf{v}_C)\delta\boldsymbol{\lambda}_E \\ \delta\dot{\boldsymbol{\lambda}}_E = \delta\boldsymbol{\omega}_E - S(\boldsymbol{\omega}_C)\delta\boldsymbol{\lambda}_E \end{cases}$$

(2.9)

where the matrices

$$\begin{aligned} A_x &= \tfrac{\partial}{\partial x}[\mathcal{F}(x,y) + \mathcal{G}(x)\mathcal{H}(x,z)], \\ B &= \tfrac{\partial}{\partial z}[\mathcal{G}(x,y)\mathcal{H}(x,z)], \end{aligned}$$

are computed at equilibrium values. Throughout the rest of the paper, the symbol $\mathcal{G}_l(\alpha_c)$ denotes the linearized time-invariant system with realization (2.9) determined by the parameter α_c.

3 Guidance/Control System

Suppose that associated to each linearized system $\mathcal{G}_l(\alpha_c)$ there is a linear time-invariant controller $\mathcal{K}(\alpha_c)$ that stabilizes and achieves adequate performance for the closed-loop system, as evaluated by some performance criterion. Theoretically, it is then possible to define a gain-scheduled controller $\mathcal{C}$ that recruits the appropriate linear controller $\mathcal{K}(\alpha)$ based on the measured value α of the parameter α_c.

In practice, $\mathcal{C}$ is obtained by designing a family of linear controllers for a *finite* number of systems $\mathcal{G}_l(\alpha_c)$, and interpolating between these controllers to achieve adequate performance for all linearized plants in the regimes where the vehicle is expected to operate. During real time operation, the controller parameters are updated as functions of the scheduling variable $\alpha = [\mathbf{V}_T, \dot{\psi}, \gamma]'$.

3.1 Linear Controller Design

The methodology selected for linear control system design was $\mathcal{H}_\infty$ ["Doyle (1989)"]. This method rests on a firm theoretical basis, and leads naturally to an interpretation of control design specifications in the frequency domain. Furthermore, it provides clear guidelines for the design of controllers so as to achieve robust performance in the presence of plant uncertainty.

The first step in the controller design procedure is the development of a synthesis model which can serve as an interface between the designer and the $\mathcal{H}_\infty$ controller synthesis algorithm. Consider the feedback system shown in figure 3.1, where $\mathcal{G}_l(\alpha_c)$ is obtained from the linearized model of the AUV and $\mathcal{K}(\alpha_c)$ is the controller to be designed. The correspondence between the standard notation of figure 3.1 ["Doyle (1992)"] and that introduced in Section 2 for incremental variables will be clear form the context. The block $\mathcal{J}(\alpha_c)$ within the dashed line is the synthesis model, which is derived from the linearized model of the plant by appending the depicted weights. In practice, the weights serve as tuning "knobs" which the designer can adjust to meet the desired performance specifications.
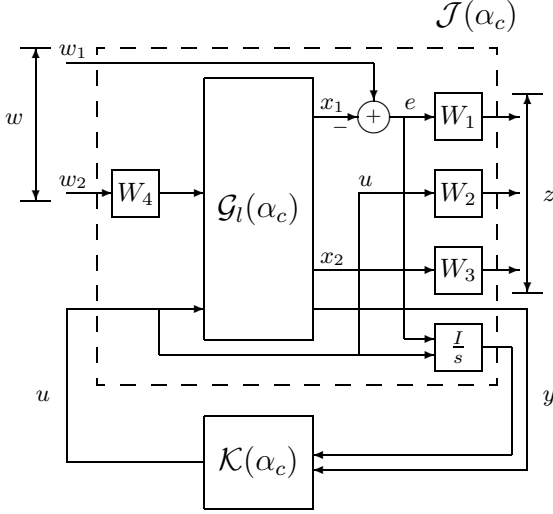
Figure 3.1: Synthesis model.

The signal w_1 corresponds to the vector of input commands that must be tracked. In this design example, it includes linear positions. The signal w_2 represents the noise inputs to each of the sensors, and disturbance inputs to the states of the plant. The signal u corresponds to the control inputs to the system. The signal x_1 represents the components of the state vector that must track the input commands, while the vector x_2 contains the remaining state variables that must be weighed.

The outputs of W_1, W_2, and W_3 constitute the vector z. Since zero steady-state error in tracking the step command for all variables in x_1 was required, the weighting function W_1 was chosen as a diagonal of integrators. The integrator gains were adjusted to get desired command response bandwidths. The weights W_3, W_4 do not include any dynamics. In order to drive $\delta_{a,c}$ to zero in steady state, an integrator was included in W_2. The signal y includes all the states of the plant $\mathcal{G}_l(\alpha_c)$, together with the appended integrator states that correspond to integrators.

Given a design model, suppose that the feedback system is well posed and let $\mathcal{T}_{zw}$ denote the closed loop transfer matrix from w to z. The $\mathcal{H}_\infty$ synthesis problem consists of finding, among all controllers that yield a stable closed loop system, a controller $\mathcal{K}(\alpha_c)$ that minimizes the maximum energy gain of the closed loop operator $\mathcal{T}_{zw}$, denoted $||\mathcal{T}_{zw}||_\infty$. This problem was solved using the methodology exposed in ["Khargonekar (1985)"], see ["Silvestre (1994)"].

3.2 Non-linear Tracking Controller Implementation

A set of controllers was determined for a finite combination of values of $\mathbf{V}_T, \dot{\psi}$ and γ, and their parameters interpolated according to the scheduling vector α in a fixed bounded domain, see ["Silvestre (1994)"]. The implementation of the resulting non-linear gain scheduled controller was done by extending the D-methodology described in ["Kaminer (1993)"], which guarantees the following fundamental *linearization property*: the linearization of the nonlinear feedback control system about each equilibrium trajectory preserves the internal
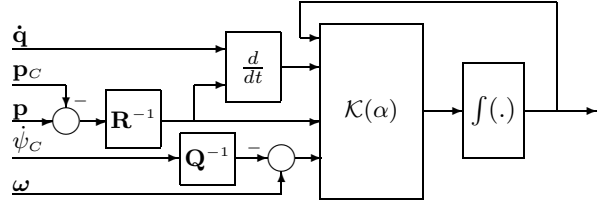

Figure 3.2: Tracking controller implementation

as well as the input-output properties of the corresponding linear closed loop designs.

Surprisingly, this property is often not satisfied by gain scheduled controllers proposed in the literature, see ["Kaminer (1993)"] and the references therein. In practice, violation of that property may lead to degradation in performance, or even instability, of the closed-loop system.

The D-methodology is based on the key observation that linear controllers are designed to operate on the perturbations of the plant's inputs and outputs about the equilibrium points. Proper blending of the different controllers requires that they have access to such perturbations, locally. This is achieved by differentiating some of the measured outputs before they are fedback to the gain scheduled controller. In order to preserve the input-output behaviour of the feedback system, integral action is provided at the input to the plant.

The gain scheduled controller implementation is depicted in figure 3.2, where $\mathcal{K}$ denotes the interpolation of the linear controllers obtained in Subsection 3.1. Notice that *the only external commands to the trajectory tracking controller are $\mathbf{p}_C$ and $\dot{\psi}_C$*, which are easily available from the trajectory generator.

It is important to stress that the D-method presented above requires differentiating some of the plant's measured outputs. Except for the case where some of the derivatives are available from dedicated sensors, this cannot be done in practice. In this case, the differentiation operator may simply replaced by a causal system with transfer function $\frac{s}{\tau s + 1}$, or by a simple finite difference operator for discrete-time implementation, see ["Kaminer (1993)"]. It is also important to remark that the D-methodology would require that the time-derivative of $\dot{\boldsymbol{\lambda}}_E$ be computed on-line. However, from the relations $\ddot{\mathbf{q}}_E = \ddot{\mathbf{q}}$ and $\dot{\boldsymbol{\lambda}}_E = \boldsymbol{\omega} - \mathbf{Q}\dot{\boldsymbol{\lambda}}_C$, it follows that the derivative is simply computed as depicted in figure 3.2. Thus, the method proposed avoids the need to feedforward trimming conditions for the state variables and inputs, except $\mathbf{p}_C$ and $\dot{\psi}_C$.

4 Navigation System Design

This section describes the basic framework used in the design of the navigation system for the AUV MARIUS. The objective of this system is to obtain accurate estimates of the position and attitude of the vehicle, based on measurements available from a motion sensor package installed on-board. The estimates are input to the integrated control and guidance systems described in Section 3.

This paper adopts a conceptually simple framework for filtering that is rooted in the kinematic equations of (2.3) This approach is based on the theory of *complementary filtering*, see ["Lin (1991)"] for an introduction to the subject and ["Oliveira (1994)"] for a complete study of the multi-rate case.

4.1 Attitude Estimation

The motion sensor package of MARIUS includes two *pendulums* and one *fluxgate* that provide - indirectly - measurements $\boldsymbol{\lambda}_m$ of $\boldsymbol{\lambda}$, and three *rate gyroscopes* that provide measurements $\boldsymbol{\omega}_m$ of angular body rates $\boldsymbol{\omega}$.

For the sake of completeness, the synthesis of a continuous-time filter to estimate pitch based on measurements of pitch and pitch rate is briefly described below. This illustrative example is simple, yet it captures the essence of complementary filter design.

The simplified design model is depicted in figure 4.1, where $\dot{\theta}$ denotes the time derivative of θ and $\dot{\theta}_m$ is the measured value of $\dot{\theta}$. The measurements θ_m and $\dot{\theta}_m$ are corrupted by observation noise $\boldsymbol{\nu}$ and process noise ξ respectively, where the latter is obtained by driving an integrator with a noise source $\boldsymbol{\mu}$. Clearly, this simple model includes the case where the measurement $\dot{\theta}_m$ of $\dot{\theta}$ exhibits an unknown bias term that must be rejected.
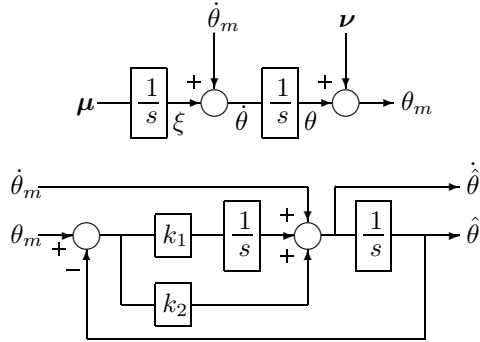

Figure 4.1: Complementary Filter - Design model and Implementation

The design model admits the description

$$\dot{\mathbf{x}} = F\mathbf{x} + G_u\mathbf{u} + G_\mu\boldsymbol{\mu},$$
$$\mathbf{z} = H\mathbf{x} + \boldsymbol{\nu},$$

where $\mathbf{x} = [\xi, \theta]'$ is the state vector, $\mathbf{u} = \dot{\theta}_m$ and $\mathbf{z} = \theta_m$ are input and output variables, respectively, and F, G_u, G_μ and H are matrices of compatible dimensions. Following the standard approach in the design of Kalman filters, it is assumed that $\boldsymbol{\mu}$ and $\boldsymbol{\nu}$ are zero mean, gaussian, uncorrelated stochastic processes with covariances

$$E[\boldsymbol{\mu}(t)\boldsymbol{\mu}(\tau)] = Q\delta(t-\tau), \ E[\boldsymbol{\nu}(t)\boldsymbol{\nu}(\tau)] = R\delta(t-\tau),$$

where $\delta(.)$ is the Kronecker delta operator. Under some generic technical assumptions, the stationary

filter that minimizes the mean-square error estimation of $\mathbf{x}$ based on the observations $\mathbf{z}$, is asymptotically stable, and given by the Kalman filter structure

$$\dot{\hat{\mathbf{x}}} = F\hat{\mathbf{x}} + G_u\mathbf{u} + K(\mathbf{z} - H\hat{\mathbf{x}}),$$

where $\hat{\mathbf{x}}$ denotes the best estimate of $\mathbf{x}$, and

$$K = [k_1, k_2]' = PH^T R^{-1}$$

is obtained from the positive semidefinite solution P to the algebraic Riccati equation

$$FP - PF^T - PH^T R^{-1} HP + G_\mu Q G_\mu^T = 0.$$

The resulting filter is depicted in figure 4.1. Let $\mathcal{T}_{\hat{\theta},d}$ and $\mathcal{T}_{\hat{\theta},i}$ denote the operators from θ_m to $\hat{\theta}$ and *from the integral of $\dot{\theta}_m$* to $\hat{\theta}$, respectively. Straightforward computations show that the corresponding - stable - transfer functions are given by

$$T_{\hat{\theta},d}(s) = \frac{sk_2 + k_1}{s^2 + sk_2 + k_1}, \ T_{\hat{\theta},i}(s) = \frac{s^2}{s^2 + sk_2 + k_1},$$

and that

$$T_{\hat{\theta},d}(s) + T_{\hat{\theta},i}(s) = I. \tag{4.1}$$

Equation (4.1) admits a simple interpretation: in order to compute estimates of angular position $\hat{\theta}$, the filter complements the information θ_m available directly from the pendulum at low frequency with that obtained by integrating the information from the rate gyro at high frequency. Thus, the filter is convenient to use when high frequency sensor data of good quality are available. Notice also that with the above filter structure, any bias in the rate information will be rejected at the output.

From a purely formal point of view, if the variable θ_m in figure 4.1 is redefined as the integral of the input $\mathbf{u} = \dot{\theta}_m$, then the overall filter defines an input-output operator from $\mathbf{u}$ to $[\dot{\hat{\theta}}, \hat{\theta}]'$ that is equal to $[I, \frac{I}{s}]'$, thus capturing the underlying physical constraint between angular velocity and position. This seemingly trivial property plays an important role in the stability analysis of combined controller and navigation systems, since in theory no extra dynamics are introduced in the overall loop by the complementary filter. In practice, high frequency dynamics are bound to be introduced in that loop, as one must use a high bandwidth low pass filter to process the information obtained from the rate gyro. However, well known results from robust stability theory indicate that stability will not be compromised if one restricts the bandwidth of the control loop to be well bellow that of the corresponding complementary filter, see ["Doyle (1992)"] for the general theory and ["Oliveira (1994)"] for an application to the vehicle under study.

The following requirements were specified in the design example reported here: i) pitch and pitch rate estimation errors should be driven asymptotically to zero when the vehicle is following a trajectory with zero angular acceleration (in particular, the filter should reject constant rate gyro bias terms); ii) the filter bandwidth corresponding to the transfer function from pitch measurement to

the corresponding estimate should be on the order of 0.3 rad/s (this requirement is dictated by the low pass sensor characteristics); iii) the overall bandwidth of the filter after insertion of a low pass system at the output of the rate gyro should be on the order of $30 rad/s$, that is, much larger than that of the corresponding control loops.

Using the formalism exposed above in a discrete-time setting, the covariances Q and R were manipulated to shape the transfer functions between the variables $\mathbf{z}$ and $\mathbf{u}$ and the estimates $\hat{\mathbf{x}}$ of $\mathbf{x}$. The resulting complementary filter, sampled at $50Hz$, exhibits the Bode diagram of figure 4.2. A low pass filter $\mathcal{F}$ with a bandwidth of $30 \, rad/s$ has been inserted at the output of the rate gyro. Notice how the pitch estimator relies on the information provided by the pendulum at low frequency. At high frequency, the estimator relies essentially on the integral of measured pitch rate.
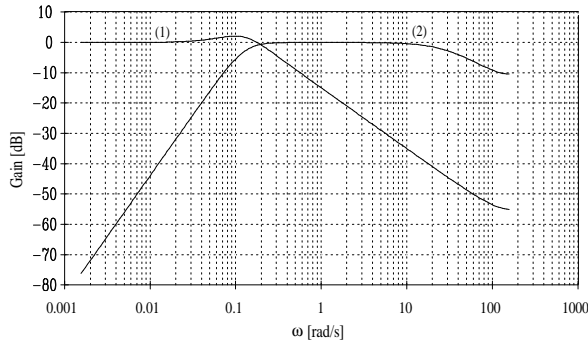

Figure 4.2: Discrete Bode diagrams corresponding to the operators: (1) - $\mathcal{T}_{\hat{\theta},d}$, (2) - $\mathcal{T}_{\hat{\theta},i}\mathcal{F}$.

The general case (where corrected estimates of roll, pitch and yaw angles and body rates are sought) can be dealt with by an obvious generalization of the above procedure ["Oliveira (1994)"].

4.2   Position/Velocity Estimation

The following sensor units are used to provide measurements of the linear position and velocity of the vehicle: a *long baseline positioning system* (LBL) and a *depth cell* that provide measurements $\mathbf{p}_m$ of $\mathbf{p}$, and a Doppler sonar that provides measurements of the velocity of the vehicle with respect to the water (i.e., of $\mathbf{v} - \mathbf{R}^{-1}\mathbf{v}_w$, where $\mathbf{v}_w$ is inertial sea current velocity).

Conceptually, the basic framework described in Section 4.1 could be used to design a filter that would provide corrected estimates of the position and velocity of the vehicle with respect to the water and to the seabed. In fact, the time-derivative of $\mathbf{p}$ can be estimated from $\mathbf{v}$ using the kinematic equations. A time-invariant, multivariable complementary filter, could then be obtained adopting a design model similar to that in figure 4.1.

Notice, however, that due to the characteristics of the acoustic channel, the measurements from the LBL system are available at a rate that is much smaller than that of the remaining sensors. Thus, the resulting filter must exhibit a multi-rate structure. This problem has been tackled and solved in ["Oliveira (1994)"] exploring the relationship between multi-rate and periodic systems,

and using some algebraic and analytical results on the equivalence between (discrete-time) periodic and time-invariant systems ["Bittanti (1990)", "Khargonekar (1985)", "Souza (1991)"].
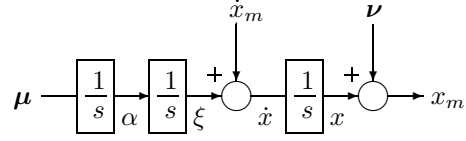

Figure 4.3: Complementary Filter - Design model

The set-up adopted is best explained by considering the simplified case where only navigational data along the inertial $x-$ axis are sought. The corresponding filter design model is depicted in figure 4.3, where $\dot{x}$ denotes the time derivative of x and $\dot{x}_m$ is the measured value of $\dot{x}$ that is derived from the Doppler log output. The measurements x_m and $\dot{x}_m$ are corrupted by observation noise $\boldsymbol{\nu}$ and process noise ξ respectively, where the latter is obtained by driving a double integrator with a noise source $\boldsymbol{\mu}$. The state variable ξ captures the evolution of the water current in the $x-$ direction.

Suppose that measurements x_m and $\dot{x}_m$ are available at rates $\frac{1}{MT}$ and $\frac{1}{T}$ respectively, where $\frac{1}{T}$ is the fastest sampling rate and M is an integer. By discretizing the above design model at the sampling frequency of $\frac{1}{T}$, an M-periodic, discrete-time design model is obtained which is described by [1]

$$\begin{aligned} \mathbf{x}(k+1) &= F(k)\mathbf{x}(k) + G_u(k)\mathbf{u}(k) + G_\mu(k)\boldsymbol{\mu}(k) \\ \mathbf{z}(k) &= H(k)\mathbf{x}(k) + \boldsymbol{\nu}(k), \end{aligned} \quad (4.2)$$

where $\mathbf{x} = [\alpha, \xi, x]'$ is the state vector, $\mathbf{u} = \dot{x}_m$ and $\mathbf{z} = x_m$ are input and output variables, and F, G_u and G_μ are matrices of compatible dimensions. The matrix $H(k)$, which consists of a string of zeros and ones, mirrors the position interrogation strategy. It is easy to check that $H(k + M) = H(k)$. Assume that the state and observations are corrupted by zero mean, gaussian, white noise processes with covariance matrices

$$\begin{aligned} E[\boldsymbol{\mu}(k)\boldsymbol{\mu}(j)^T] &= Q(k)\delta((k-j)modM) \\ E[\boldsymbol{\nu}(k)\boldsymbol{\nu}(j)^T] &= R(k)\delta((k-j)modM), \end{aligned} \quad (4.3)$$

where $\delta(.)$ is the Kronecker delta operator, $Q(k) \geq 0$ and $R(k) > 0$.

Associated with the periodic design model, we consider the Kalman filter structure described by

$$\begin{aligned} \hat{\mathbf{x}}(k+1) &= F(k)\hat{\mathbf{x}}(k) + G_u(k)\mathbf{u}(k) \\ &\quad + K(k)\left[\mathbf{z}(k) - H(k)\hat{\mathbf{x}}(k)\right], \end{aligned} \quad (4.4)$$

where the Kalman gain $K(k)$ is given by

$$K(k) = P(k)H^T(k)\left[H(k)P(k)H^T(k) + R(k)\right]^{-1}, \quad (4.5)$$

and the matrix $P(k)$ is the unique periodic, symmetric, positive-semidefinite stabilizing solution to

---

[1]In the matrix parameters, k is used as the periodic index ($k \, mod \, M$).

the periodic Riccati equation

$$\begin{aligned} P(k+1) \ = \ & F(k)P(k)F^T(k) + G_u(k)Q(k)G_u^T(k) \\ & -F(k)P(k)H^T(k)\left[H(k)P(k)H^T(k)\right. \\ & \left.+R(k)\,\right]^{-1} H(k)P(k)F^T(k). \qquad (4.6) \end{aligned}$$

The technical conditions under which such a periodic solution exists can be found in ["Souza (1991)"]. The resulting multi-rate complementary filter is depicted in figure 4.4. The filter complements the information obtained from the LBL system at low frequency, with that obtained from the Doppler log at high frequency. Furthermore, the filter rejects any possible biases caused by the non-zero velocity of the water with respect to the seabed.

It is important to point out that numerically efficient methods to solve the periodic Ricatti equation (4.6) are available. A good reference is the work of ["Bittanti (1990)"], which explores the equivalence between the class of periodic systems and a subclass of invariant systems using a certain *lift* operator. The reader will find in ["Oliveira (1994)"] the application of this circle of ideas to the design of a multi-rate filter for the AUV MARIUS based on information provided by the LBL system and the Doppler sonar.
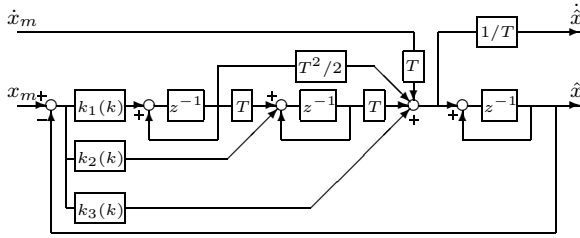

Figure 4.4: Multi-Rate Complementary Filter

In the case where navigational data along x, y, z - axes are required, a simple extension of the above design procedure leads to the general navigation system of figure 4.5, where $\mathcal{M}$ consists of three multi-rate complementary filters with the structure shown in figure 4.4. For simplicity of presentation, it was assumed that $\mathbf{v}_w = 0$.

Interestingly enough, the multi-rate filters described exhibit properties that are the generalization of those obtained for the single-rate case, as explained briefly in the following.
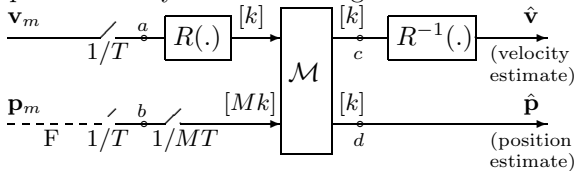
$\mathcal{M}$ - multi-rate filter; $[k]$ - time mark;
M - integer; F - fictitious sampler.

Figure 4.5: Multi-Rate Navigation System.

Let $\mathcal{G}$ be the time-varying operator from a to c that is obtained by forcing b to be equal to the discrete-time integral of a. It has been checked computationally in ["Oliveira (1994)"] that for certain combinations of sampling frequencies, it is possible to select the process and noise covariances

in (4.3) such that the operator can be written in the form $\mathcal{G} = I + \Delta$, where the induced norm ["Doyle (1992)"] of the operator Δ is small. Mathematically, this means that $\mathcal{G}$ is close to the desired identity operator. As in the time-invariant case, this property plays a key role in analyzing the stability of combined navigation, guidance and control systems, and suggests important rules of thumb for the choice of the covariance matrices in (4.3). The theory required for the analysis borrows from well known results in the area of robust stability of time-varying systems. The algorithms for computing the induced norm of Δ are described in ["Oliveira (1994)"].

5 Integrated Navigation, Guidance and Control.

The combined performance of guidance, navigation and control was evaluated in simulation with a nonlinear model of the vehicle. The simulation included physically based models of the sensor units described in Section 4. In the simulations, the control and navigation systems were discretized using the following sampling rates:

- Navigation (Attitude and attitude rates): $50\ Hz$, that is, larger than twice the desired bandwidth of the corresponding complementary filters.

- Navigation (Linear position and velocity) - LBL system: $0.2\ Hz$, Doppler sonar: $1\ Hz$. These frequencies are mission dependent, and reflect the compromise among such factors as range of operation required, precision sought and (acoustic) energy minimization.

- Integrated Control and Guidance - $10Hz$, to avoid potential aliasing introduced by the attitude navigation system.

The reference for linear position in the $x - y$ plane is an $\mathcal{S}$ - shaped trajectory consisting of three straight lines $50m$ long each, and two semicircumferences with radii of $38m$. The reference trajectory in the vertical plane descends smoothly along the depth coordinate z with a slope of -10 deg. In order to simplify the interpretation of the simulation results, the trajectory was generated with a constant velocity $\mathbf{V}_T = 2.0m/s$.

The desired and observed trajectories are depicted in figure 5.1. The activity of some relevant state variables are condensed in figure 5.2. In this simulation, the LBL system uses four transponders located in positions $\{-40, 0, 160\}, \{130, 0, 150\}, \{-40, 190, 170\}$ and $\{140, 190, 135\}$, specified in meters.

At the beginning of the maneuver, the actuation variables are essentially constant during the first $25s$. Upon entering the circular path, the rudder deflects to create a torque that will impart the desired rotational speed to the vehicle. Once the desired speed is reached, the rudder deflects slightly in the opposite direction to stabilize the rotation. This maneuver is characteristic of vehicles that are unstable in yaw.
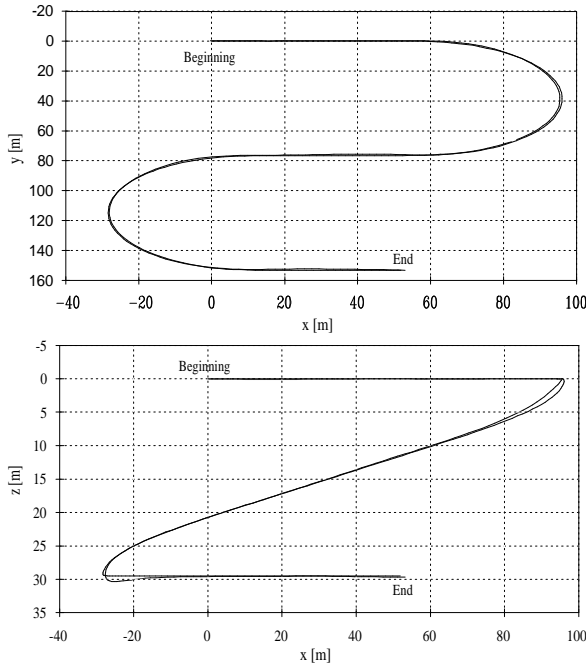
Figure 5.1: Reference and observed trajectory - horizontal and vertical planes.

At the middle of the first turn, the vehicle shows a pronounced rotation in pitch in order to converge rapidly to the desired vertical inclination of $-10deg$. This rotation is achieved by deflecting the common aileron $\delta_{a,c}$ and the elevator δ_e in opposite directions, so as to generate a pure torque. When the vehicle reaches the desired orientation, $\delta_{a,c}$ and δ_e decrease. However, their values don't tend to zero, since they must counteract the restoring torque due to the combined effects of buoyancy and gravity.

When the vehicle reaches the end of the first turn, there is a strong deflection in the rudder to drive the velocity of rotation to zero. Similar comments apply to the remaining part of the trajectory.

It is important to remark that the thrust activity rises during maneuvers that require large deflection of the control surfaces. This is required to counteract the increase in drag, which tends to slow down the vehicle.

References

["Bittanti (1990)"] Bittanti, P., Colaneri,P. and Nicolau, G. (1990). "An Algebraic Riccati Equation for the Periodic Prediction Problem," *Systems and Control Letters*, pp. 71–78.

["Doyle (1989)"] Doyle, J., Glover, K., Khargonekar, P. and Francis, B. (1989). "State space solutions to standard $\mathcal{H}_2$ and $\mathcal{H}_\infty$ control problems," *IEEE Transactions on Automatic Control*, AC- 34(8), August 1989,pp. 831–847.

["Doyle (1992)"] Doyle, J., Francis, B. and Tannenbaum, A. (1992). *Feedback Control Theory*, MacMillan Publishing Company.

["Fryxell (1994)"] Fryxell, D. and Pascoal, A. (1994). "Modeling, Identification and Control of the AUV MARIUS," *SOUV-Technical Report,* Institute for Systems and Robotics.
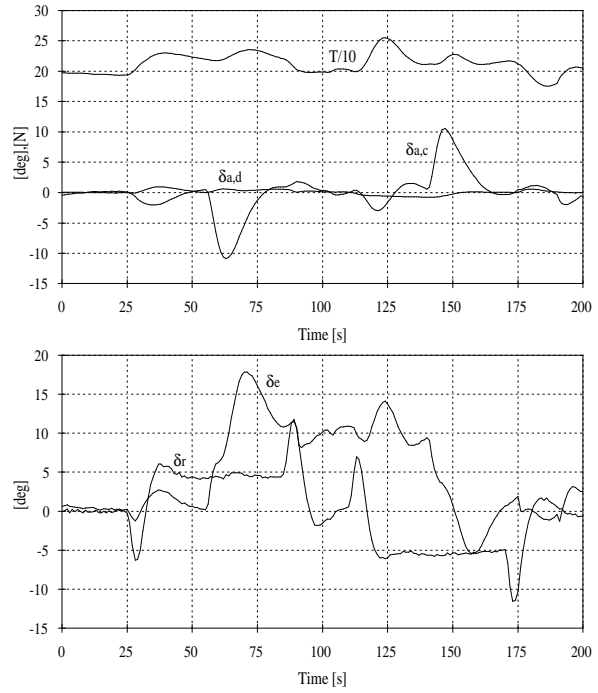
Figure 5.2: Control activity: Rudder (δ_r), Ailerons ($\delta_{a,c}$ and $\delta_{a,d}$), Elevator (δ_e) and Thruster (T).

["Healey (1993)"] Healey, A. and Lienard, D. (1993). "Multivariable sliding mode control for autonomous diving and steering of unmanned underwater vehicles," *IEEE Journal of Oceanic Engineering,* Vol. 18, N0.3, July , pp. 327-339.

["Kaminer (1993)"] Kaminer, I., Pascoal, A., Khargonekar, P. and Thompson, C. (1993). "A Velocity Algorithm for the Implementation of Non-Linear Gain-Scheduled Controllers," Proc. 1993 European Control Conference, pp. 787-792. Full paper version accepted for publication in *Automatica*.

["Khargonekar (1985)"] Khargonekar, P., Poola, K. and Tannenbaum, A. (1985). "Robust Control of Linear Time-Invariant Plants using Periodic Compensation," *IEEE Transactions on Automatic Control,* Vol. AC-30, pp.1088–1096.

["Lin (1991)"] Lin, C. (1991). *Modern Navigation, Guidance, and Control Processing*, Prentice-Hall.

["Oliveira (1994)"] Oliveira, P., Pascoal, A. and Silvestre, C. (1994). "Guidelines for the Design of Advanced Navigation Systems for AUVs," *SOUV-Technical Report,* Institute for Systems and Robotics.

["Pascoal (1994)"] Pascoal, A. (1994)." The AUV MARIUS: Mission Scenarios, Vehicle Design, Construction and Testing," *Proceedings of the 2nd Workshop on Mobile Robots for Subsea Environments*, Monterey Bay Aquarium, Monterey, California, USA, May.

["Silvestre (1994)"] Silvestre, C., Pascoal, A. and Kaminer, I. (1994). "Design of Integrated Guidance and Control Systems for AUVs" *SOUV-Technical Report,* Institute for Systems and Robotics.

["Souza (1991)"] Souza, C. (1991). "Periodic strong solution for the optimal filtering problem of linear discrete-time periodic systems," *IEEE Transactions on Automatic Control*, AC-36(3), pp. 333–337.